First principles modeling of exciton-polaritons in polydiacetylene chains

Antonios M. Alvertis (iD), Raj Pandya (iD), Claudio Quarti, Laurent Legrand, Thierry Barisien, Bartomeu Monserrat (iD), Andrew J. Musser (iD), Akshay Rao (iD), Alex W. Chin (iD), and David Beljonne (iD)

View Online   Export Citation   CrossMark

First principles modeling of exciton-polaritons in polydiacetylene chains

View Online   Export Citation   CrossMark

Antonios M. Alvertis,[1,a] Raj Pandya,[1] Claudio Quarti,[2,3] Laurent Legrand,[4] Thierry Barisien,[4] Bartomeu Monserrat,[1,5] Andrew J. Musser,[6] Akshay Rao,[1] Alex W. Chin,[4] and David Beljonne[2,b]

AFFILIATIONS

[1] Cavendish Laboratory, University of Cambridge, J. J. Thomson Avenue, Cambridge CB3 0HE, United Kingdom

[2] Laboratory for Chemistry of Novel Materials, University of Mons, Place du Parc, 20, B-7000 Mons, Belgium

[3] Universite de Rennes, ENSCR, INSA Rennes, CNRS, ISCR (Institut des Sciences Chimiques de Rennes) - UMR 6226, F-35000 Rennes, France

[4] Sorbonne Universite, CNRS-UMR 7588, Institut des NanoSciences de Paris, INSP, 4 Place Jussieu, F-75005 Paris, France

[5] Department of Materials Science and Metallurgy, University of Cambridge, 27 Charles Babbage Road, Cambridge CB3 0FS, United Kingdom

[6] Department of Chemistry and Chemical Biology, Cornell University, Ithaca, New York 14853, USA

Note: This paper is part of the JCP Special Topic on Excitons: Energetics and Spatio-Temporal Dynamics.
[a] Author to whom correspondence should be addressed: ama80@cam.ac.uk
[b] Electronic mail: David.BELJONNE@umons.ac.be

ABSTRACT

Exciton-polaritons in organic materials are hybrid states that result from the strong interaction of photons and the bound excitons that these materials host. Organic polaritons hold great interest for optoelectronic applications; however, progress toward this end has been impeded by the lack of a first principles approach that quantifies light–matter interactions in these systems, which would allow the formulation of molecular design rules. Here, we present a theoretical framework that combines first principles calculations for excitons with classical electrodynamics in order to quantify light–matter interactions. We exemplify our approach by studying variants of the conjugated polymer polydiacetylene, and we show that a large polymer conjugation length is critical toward strong exciton–photon coupling, hence underlying the importance of pure structures without static disorder. By comparing to our experimental reflectivity measurements, we show that the coupling of excitons to vibrations, manifested by phonon side bands in the absorption, has a strong impact on the magnitude of light–matter coupling over a range of frequencies. Our approach opens the way toward a deeper understanding of polaritons in organic materials, and we highlight that a quantitatively accurate calculation of the exciton–photon interaction would require accounting for all sources of disorder self-consistently.

Published under license by AIP Publishing. https://doi.org/10.1063/5.0019009

I. INTRODUCTION

Excitons are bound electron–hole pairs that appear in semiconductors and are critical to the optoelectronic response of these materials. These quasiparticles are connected to a finite oscillating polarization that emits an electromagnetic wave, which can act on an incident wave, leading to a light–matter interplay. Once a photon is close to resonance with an exciton, light–matter coupling can become strong, and the two cannot be treated independently, as it was first realized in the pioneering works of Pekar[1,2] and Hopfield[3]

more than six decades ago. This coupling between polarization and photons is captured by introducing the quanta of a new quasiparticle referred to as a polariton, which describes the propagation of electromagnetic energy in matter.[4]

Organic semiconductors are a class of materials, the light–matter interactions of which are relevant to a number of promising optoelectronic applications, making the understanding of their polariton properties interesting from a technological point of view. Their applications include light-emitting diodes (LEDs),[5] solar cells,[6] and room temperature polariton lasers.[7,8] Excitons in

organic semiconductors are typically strongly bound[9,10] Frenkel-like excitons,[11–14] and their dispersion can be considered to be approximately flat[15] compared to the strong dispersion of light, as visualized in Fig. 1. For an incident photon close to resonance with an exciton state of an organic semiconductor, strong coupling leads to two new polariton states that are referred to as upper polariton (UP) and lower polariton (LP), respectively. As depicted in Fig. 1, this results in a stop-band (shaded region), where no light propagation takes place within the material. The width Δ of the stop-band depends on the magnitude of the exciton–photon interaction. The stop-band is also related to, but is distinct from, the so-called Rabi splitting that is commonly used to quantify light–matter interactions, which is defined as the maximal vertical distance between the upper and lower polariton branches.[16] Polaritons in organic semiconductors have often been studied for molecular systems placed between highly reflecting mirrors that confine incident light.[8,17–20] This microcavity effect leads to a standing electromagnetic wave that interacts with the material system. However, here we focus on the case of unconfined photons, and not on such microcavity polaritons.

The building block of organic semiconductors is often organic molecules, the large size and weak intermolecular van der Waals interactions of which lead to phonon modes with low frequencies; hence, they are strongly activated at room temperature. These slow nuclear motions lead to large variations of the electronic interactions between neighboring molecules.[21,22] Since excitons can spatially extend over several molecules,[23,24] such low-energy phonons can have a strong influence on their properties.[25] Similarly, organic semiconductors based on conjugated polymers exhibit very low-frequency phonon modes that are strongly coupled to their excitons.[26] However, it is not only vibrations of low energies that couple strongly to excitons, as in organic systems high-frequency motions such as carbon–carbon stretches have often been discussed to dominate this interaction.[27,28] This strong coupling of excitons to the
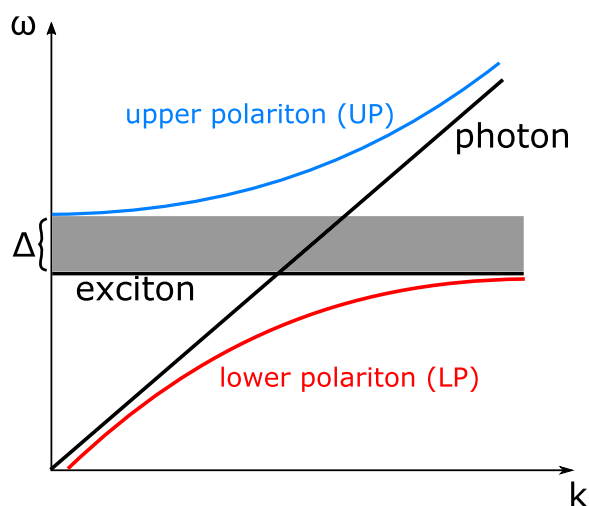
vibrations of organic semiconductors is expected to also have an impact on exciton–photon coupling, and indeed it has been shown that vibrations have a strong effect on the dynamics of polariton states.[29–33]

Therefore, understanding the properties of polaritons requires accounting not only for exciton–photon but also exciton–vibration interactions, through a Hamiltonian operator of the form
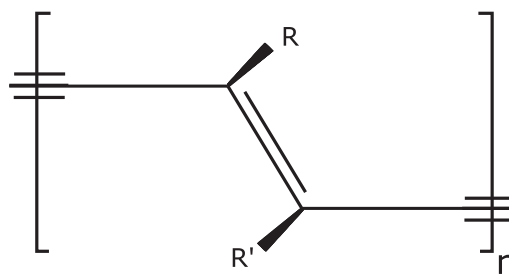
$$H = H_{\text{exc-ph}} + H_{\text{exc-vib}}, \tag{1}$$

where the operator $H_{\text{exc-vib}}$ describes the exciton–vibration interactions. For a single exciton state with energy ω_{exc}, coupled to a photon of energy ω_{ph}, the exciton–photon Hamiltonian can be written within the so-called resonance approximation[34]

$$H_{\text{exc-ph}} = \omega_{\text{ph}}\hat{a}^\dagger\hat{a} + \omega_{\text{exc}}\hat{c}^\dagger\hat{c} - ig(\hat{a}\hat{c}^\dagger - \hat{a}^\dagger\hat{c}). \tag{2}$$

Here, $a^\dagger$ (a) is the creation (annihilation) operator of the photon state, and $c^\dagger$ (c) is the creation (annihilation) operator of the exciton. The constant g quantifies the magnitude of the exciton–photon interaction and is related to the width of the stop-band Δ of Fig. 1 via the relationship: $g = \frac{1}{4}\sqrt{\omega_{\text{ph}}\Delta}$.

While first principles approaches have been used in several cases to parameterize the exciton–vibration interactions encoded in $H_{\text{exc-vib}}$,[35,36] the same cannot be said for the exciton–photon Hamiltonian of Eq. (2). To the best of our knowledge, a comprehensive *ab initio* method for modeling the stop-band of organic systems is thus far missing. Naturally, experiment can inform computational models on the range of values of Δ; however, this does not allow for a truly predictive approach of modeling light–matter interactions in these systems. It also remains unclear how vibrational effects affect the stop-band.

Here, we develop a theoretical framework for simulating exciton–photon interactions in organic systems by combining first principles calculations for excitons with the macroscopic theory of polaritons from classical electrodynamics. We, thus, extract the stop-band width Δ that appears in the microscopic Hamiltonian (2). We exemplify our approach by studying variants of the conjugated polymer polydiacetylene (PDA) (Fig. 2), and we show that the conjugation length of the polymer chains has a large impact on the magnitude of exciton–photon interactions. Exciton properties of PDA are obtained from first principles by using accurate Green's function based methods (GW-BSE),[37–39] which are known to be appropriate for the study of conjugated polymers,[40] due to successfully capturing the large intrinsic correlation length of the electrons and holes that

FIG. 1. The dispersion of a photon in a material intersects with that of an exciton, and their interaction leads to two new hybrid polariton states. The upper and lower polaritons are separated by an energy gap of width Δ (shaded region), which is referred to as the stop-band.

FIG. 2. The structure of a diacetylene monomer, which generally coincides with the unit cell of an infinite and periodic crystal of polydiacetylene.

participate in exciton states. We compare the simulated results to experimental reflectivity measurements of the stop-band width, and we find the two to be in reasonable agreement. However, by only considering the effect of the main exciton peak on incident photons, the internal structure of the stop-band as it appears in reflectivity measurements is not reproduced in the calculation. By coupling *GW*-BSE calculations for the excitons, to non-perturbative finite differences methods for the vibrations,[41,42] we show that phonon effects have an important effect on the internal stop-band structure.

The structure of this paper is as follows. Section II provides an overview of our theoretical approach for describing light–matter interactions. We apply our methodology to disorder-free PDA in Sec. III. An overview of the studied systems is also provided in this section, alongside a discussion of their exciton properties and the experimental determination of the magnitude of light–matter interactions. We then proceed to discuss the role of static disorder in the sense of limiting the infinite conjugation length of disorder-free chains in Sec. IV. The impact of dynamic disorder (vibrations) on light–matter interactions is discussed in Sec. V, along with a detailed outline of the employed methodology for accounting for its effect. We summarize the entirety of our results and discuss potential future avenues in Sec. VI.

II. THEORETICAL BACKGROUND

Consider an electromagnetic wave **E**, **B** interacting with a material of dielectric $\varepsilon(\omega)$. The wave equation for the electric field in frequency space reads

$$\nabla^2 \mathbf{E}(\mathbf{r}, \omega) + \frac{\omega^2}{c^2} \varepsilon(\omega) \mathbf{E}(\mathbf{r}, \omega) = 0. \tag{3}$$

For the moment, and for the sake of simplicity, let us consider a bulk isotropic material, for which the electric field can be treated as a plane wave,

$$\mathbf{E}(\mathbf{r}, \omega) = E \cdot e^{i(\mathbf{k} \cdot \mathbf{r} - \omega t)}. \tag{4}$$

By substituting Eq. (4) into (3), we obtain

$$\left[-k^2 + \frac{\omega^2}{c^2} \varepsilon(\omega) \right] E \cdot e^{i(\mathbf{k} \cdot \mathbf{r} - \omega t)} = 0. \tag{5}$$

The transverse eigenmodes of the system satisfy the condition $E \neq 0$; therefore,

$$c^2 k^2 = \omega^2 \varepsilon(\omega). \tag{6}$$

It, thus, becomes obvious that if one obtains the dielectric response $\varepsilon(\omega)$ of a material, the dispersion of the light field in the material, i.e., the polariton dispersion, can be obtained by solving Eq. (6). This method is agnostic to the level at which the electronic structure is computed, and our *GW*-BSE methodology provides but one possibility.

Let us now consider the so-called resonance approximation to Eq. (6), as a useful way of gaining physical intuition on the origins of the stop-band. However, we emphasize that we do not make use of this approximation to obtain the simulated results presented in this paper, and it only serves as a way of developing intuition. Unless we are at resonance with an excited state $\omega = \omega_o$, the imaginary part of the dielectric response is negligible; therefore, Eq. (6) can be approximated as

$$c^2 k^2 = \omega^2 \text{Re}(\varepsilon(\omega)). \tag{7}$$

Equation (7) shows that there will only exist real solutions for the wavevector k once $\text{Re}(\varepsilon(\omega))$ is positive. While this is generally the case, $\text{Re}(\varepsilon(\omega))$ can become negative in the vicinity of an optical transition i with a high oscillator strength f_i. This can be seen within a Lorentz oscillator model of the dielectric response,[43]

$$\varepsilon(\omega) = \varepsilon_0 + \frac{Ne^2}{m} \sum_i \frac{f_i}{\omega_i^2 - \omega^2 - i\omega\gamma_i}. \tag{8}$$

The real part can be written as

$$\text{Re}(\varepsilon(\omega)) = \varepsilon_0 + \frac{Ne^2}{m} \sum_i f_i \frac{\omega_i^2 - \omega^2}{(\omega_i^2 - \omega^2)^2 + \omega^2 \gamma_i^2}, \tag{9}$$

where ε_0 is the background dielectric response, N is the number of molecules per unit volume, m is the electron mass, and γ_i is the dephasing rate. In the vicinity of a transition i, $\omega = \omega_i + \delta\omega$, and only keeping terms in the first order of $\delta\omega$, we obtain the condition for $\text{Re}(\varepsilon(\omega)) < 0$ to be

$$f_i > \left(1 + \frac{\omega_i}{2\delta\omega} \right) \cdot \frac{\gamma_i^2}{\omega_p^2}, \tag{10}$$

where $\omega_p^2 = \frac{Ne^2}{\varepsilon_0 m}$, the plasma frequency of a material. The width of the frequency region over which condition (10) holds and thus $\text{Re}(\varepsilon(\omega)) < 0$ defines the stop-band width Δ.

Therefore, the brighter an optical transition, the more likely it is that it will lead to a forbidden region for light propagation in the material. Since the oscillator strength of a material satisfies the sum rule

$$\sum_i f_i = Z, \tag{11}$$

with Z being the number of electrons per molecule, we conclude that materials with fewer bright optical transitions are more likely to satisfy condition (10) and lead to strong light–matter interactions. This provides the motivation for studying extended one-dimensional systems like PDA, as elaborated in Sec. III.

Before proceeding to use the presented methodology on material systems, we would like to highlight two points regarding its range of applicability. First of all, this has been discussed in the context of a general Lorentz oscillator, and the frequencies ω_i appearing in Eq. (8) need not correspond to exciton states. While here we focus on exciton-polaritons, optical phonons and plasmons can also form hybrid states with light,[44,45] and the presented theoretical framework could be used to describe such phenomena. Secondly, the polariton properties we calculate correspond to the bulk of an infinite material structure. However, these states can also form at the surface of a material, only propagating along the interface between different media. These states are referred to as surface polaritons and have a finite dispersion within the stop-band of the infinite "bulk" polariton states that we study here.[46] Our theoretical framework does not capture such surface effects but could be extended in that direction in the future.

III. APPLICATION TO DISORDER-FREE PDA

Polydiacetylene (PDA) is a conjugated polymer with an alternating sequence of single-double-single-triple carbon–carbon bonds, as visualized in Fig. 2. These materials are known to give

very high-quality crystals, with an almost perfect alignment of the polymer chains parallel to each other and free from conformational defects, due to the topochemical reaction they originate from.[47] Variants of PDA are traditionally named after the color of the transmitted light through a film of the material. Here, we study two PDA variants shown in Fig. 3, alongside their absorption and reflection spectra. We refer to the structure of Fig. 3(a) that absorbs at lower energies as "blue" PDA[48] and the one of Fig. 3(b) that absorbs at higher energies as "red."[49,50] It is important to note that the two types of PDA chains and their optical responses should in no way be associated with varying levels of disorder in their structures but are largely determined by their backbone geometries (see Fig. 4 and associated discussion).[51]

We determine the stop-band of the two PDA variants by measuring their reflectivity spectra presented in Fig. 3, for near-normal incidence of light. Details of the experimental measurements are given in Appendix A. If we were to disregard the absorption from the exciton over a finite region of frequencies, then every incident photon with an energy within the stop-band region would be reflected, giving a reflectance of $R = 1$,[52] since no propagation of light can take place within the forbidden region. However, the finite damping γ that appears in the dielectric function of Eq. (8) due to the absorption of an exciton leads to weaker reflectance and a "gap" within the forbidden region of the stop-band[4,53] [as also seen in Fig. 7(b) for a model PDA system]. Further gaps to the high reflectivity of the stop-band can appear due to disorder or additional bright exciton peaks.

Therefore, it is not always the case that one can identify the stop-band as a region of high reflectance, and its internal structure can be rich. This is the case with the reflectivity spectra of Fig. 3. Nevertheless, we can still identify the width of the stop-band as the distance of two peaks in the reflectivity spectra: the one which appears on the low-energy side of the dip due to the absorption from an exciton state, and the one for which the reflectance reaches values at least as large as the maximum of the first peak. This way of determining the stop-band is similar to previous work,[53] and strong light–matter coupling in squarylium[54] provides a particularly good example of using the reflectivity measurements to that end.

Our reflectivity measurements show that the stop-band width is 2.64 eV and 1.16 eV for the blue and red chains, respectively. We discuss the origin of this large difference between the red and blue chains with the aid of simulations below. The measured values are within the expected range, as the stop-band width has been shown to surpass values of 1 eV–2 eV in several organic materials.[53] In particular, it has been shown that for near-normal incidence of light on a lattice of aligned dipoles, values of this order of magnitude might be obtained.[53] Given the close-to-perfect alignment of the polymer chains in PDA, as well as the large oscillator strength of their lowest bright exciton state, it is not surprising that light–matter coupling is strong.

Let us now examine some of the details of the experimental reflectivity spectra. For the blue chains, the reflectance dips around the energy of the bright singlet exciton state at 1.97 eV, and a
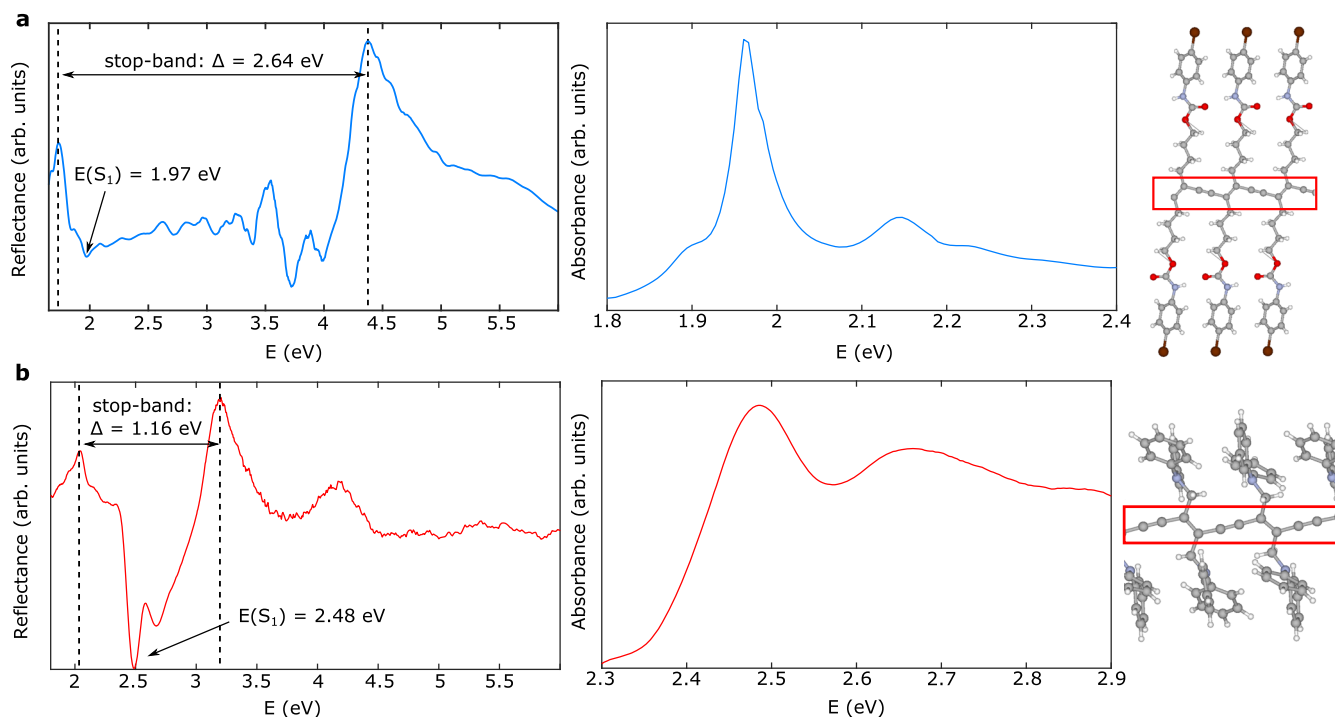
FIG. 3. Experimental reflection and absorption spectra of two studied variants of polydiacetylene: (a) blue chains and (b) red chains. The stop-band width of the two structures is approximately determined from the reflectivity spectra. The polymer structures are given alongside the experimental plots, with the polymer backbone highlighted in red rectangles, in order to distinguish it from the side-chains. Carbon atoms are denoted in light gray, hydrogen in white, oxygen in red, nitrogen in light blue, and bromine in brown.

model blue structure

model red structure
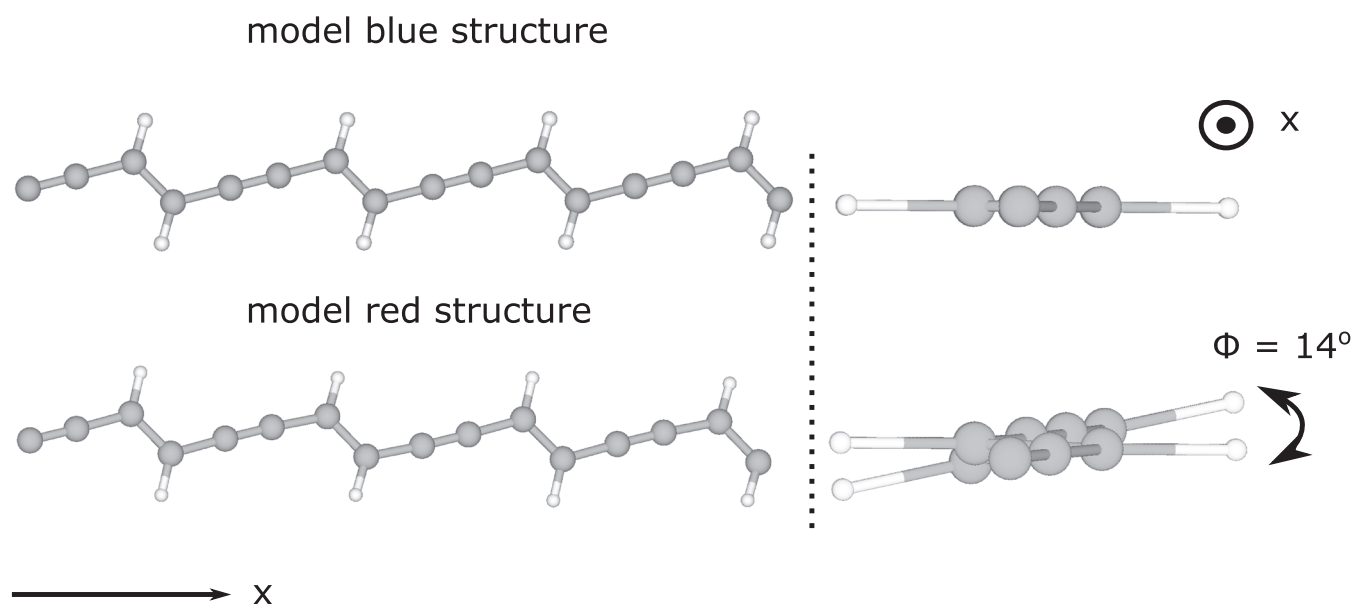
FIG. 4. Model PDA structures, constructed by substituting the side-chains of the real materials of Fig. 3 with hydrogen atoms. While the two model systems might look identical when viewed from the side (left), viewing them in the direction in which the chains lie (right) emphasizes that the blue structure is planar, while a finite torsion occurs between subsequent monomers of the red structure.

vibronic peak is also weakly resolved at 2.15 eV. Furthermore, a small dip appears at 1.85 eV, and this has been discussed to be due to minority chain populations with different geometries, which are present within the samples.[51] Additional structure appears at energies of 2.72 eV and 3.06 eV. It is currently not clear what these peaks correspond to; however, the side-chains that are connected to the conjugated PDA structure can host exciton states of their own, potentially leading to some of the observed features. At higher energies, the reflectance shows an increase at ~3.5 eV and then decreases again. This is due to exciton states of unpolymerized diacetylene monomers which are known to appear in this energy range.[51] Finally, there is a stark increase of the reflectance as photon energies approach 4.4 eV, which is then followed by a continuous drop in its value, behavior characteristic of the stop-band edge. For the red PDA, a large dip in the reflectance appears at 2.48 eV where the bright exciton state of this structure absorbs, and a vibronic peak is then present at 2.68 eV. The reflectance then increases steadily until reaching the edge of the stop-band. On the low-energy side of the main exciton peak, some additional structure is present, and similar to the case of blue PDA, we attribute this to minority chain populations.

The PDA variants of Fig. 3 contain a very large number of atoms in their unit cells, due to the size of the side-chains connected to the conjugated structure (highlighted with a red rectangle in Fig. 3). In order to understand the role of the side-chains, we resort to studying two simplified model PDA systems, where the side-chains have been substituted by hydrogen atoms, as visualized in Fig. 4. The small size of the model systems has the advantage of making the computational study of exciton–phonon interactions feasible, a fact that we return to later. When viewing the model PDA chains sideways as on the left of Fig. 4, these systems look

identical. However, by looking into the direction along which the chains extend, it becomes clear that the model red structure is not planar, and there exists a finite torsional angle of 14° between subsequent diacetylene monomers. Overall, since the interatomic distances within the polymer backbone of the four studied PDA systems are taken to be identical, the differences in their optoelectronic properties are purely due to the effects of the side-groups and the (lack of) torsion between subsequent diacetylene monomers.

The effect of this torsion has been discussed in detail previously[55] and shown to lead to significant differences in the optoelectronic response of the two systems. In crystalline PDAs, the side groups, through their mutual organization, pilot the chain conformation that in turn governs the electronic properties. However, the side groups themselves do not participate to the conjugated system, justifying the substitution by hydrogen atoms. Nevertheless, this simplification leads to a renormalization of exciton energies. This is due to the strong dielectric mismatch introduced between the conjugated chain and the outside medium, as discussed below.

The absorption of the model PDAs and real systems as computed from GW-BSE is given in Fig. 5. The computational details for the electronic structure calculations are given in Appendix B. The first thing to observe from Fig. 5 is that there is only a single bright transition for all the studied systems, at least in the idealized case of the infinite periodic material. Therefore, PDA provides an ideal system for satisfying condition (10) and observing strong light–matter interactions, since the oscillator strength is not shared between several transitions according to the sum rule of Eq. (11). It should, however, be noted that the real systems have some additional exciton states with small but non-vanishing oscillator strength at energies above 3 eV, which are associated with the side-chains.
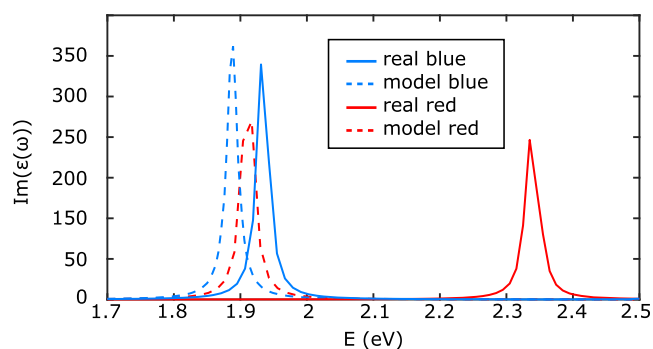
FIG. 5. Absorption of the real and model PDA chains.

TABLE I. Values for the first exciton energy $E(S_1)$, energy of the fundamental gap E_g, and exciton binding energy $E_{binding}$ of the four PDA chains.

	$E(S_1)$ (eV)	E_g (eV)	$E_{binding}$ (eV)
Real blue	1.93	3.29	1.36
Model blue	1.88	3.97	2.11
Real red	2.34	2.86	0.52
Model red	1.91	4.62	2.71

Moreover, it is interesting to note the difference in the exciton energy between the real and the respective model structures. Since the polymer backbone is identical in both cases, it is only the side-chains that can be causing the observed difference. The side-chains of the real red PDA consist of two phenyl rings, which are highly polarizable and hence provide significant screening to the Coulomb interaction that binds electron–hole pairs together. In contrast, in the model system the field lines of this Coulomb interaction are not screened by a medium, since the side-chains have been substituted by hydrogen atoms. Consequently, the exciton is more strongly bound in the model chain, further stabilizing its energy. For the real

blue system, the side-groups largely consist of non-polarizable alkyl chains; hence, the screening they provide is much weaker compared to the red PDA. This is reflected by the fact that the exciton energies of the model and real blue systems are close-to-identical, closely reproducing the experimental value from the absorption spectrum of Fig. 3(a).

Table I summarizes the values for the fundamental gaps of the chains, along with the energy of the excitons and their binding energy. The exciton binding energy of the real red and blue systems is equal to 0.52 eV and 1.36 eV, respectively, while for both model chains it is greater than 2 eV, emphasizing the large impact of the screening provided by the polarizable side-chains. This effect can be further emphasized by visualizing the exciton wavefunctions of the real and model red chains in Fig. 6. The electron density is visualized in red, for a hole fixed at the position indicated by a blue sphere. As expected, the lack of side-chain screening of the Coulomb interaction between the electron and the hole in the case of the model chain leads to an exciton that is spatially more confined than in the real system. As far as the relative electron–hole motion is concerned, we also reach a good agreement with the results from electroabsorption studies that provide an exciton Bohr radius of several nanometers, corresponding to an exciton covering a few monomer units in the blue and red conformations.[50,56]

Having obtained $\varepsilon(\omega)$ from *GW*-BSE electronic structure calculations of the three materials, we proceed to obtain the polariton dispersion. Due to the almost perfect alignment of PDA chains along one axis (x), we use the polariton dispersion relation[53]

$$c^2 k^2 = \omega^2 \varepsilon_{xx}(\omega), \qquad (12)$$

Here, $\varepsilon_{xx}(\omega)$ is the only non-zero component of the dielectric tensor of the material, and in the y and z directions, the vacuum dispersion holds: $\omega^2 = c^2 k^2$. We obtain the component $\varepsilon_{xx}(\omega)$ of the dielectric tensor, by solving the Bethe–Salpeter equation for incident light normal to the chains, which approximately emulates the experimental conditions used to obtain the reflectivity spectra of
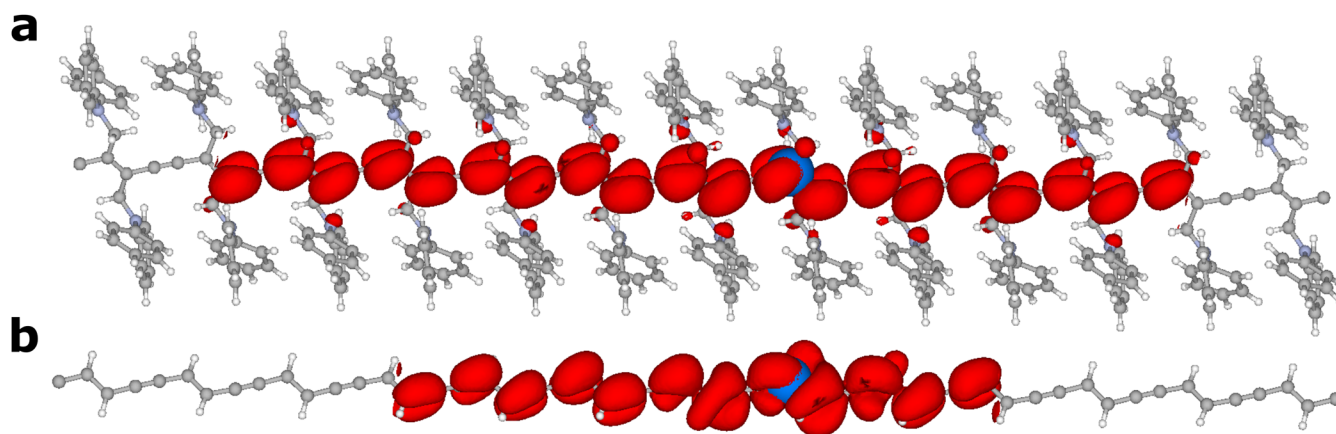

FIG. 6. Exciton wavefunction of (a) the real red PDA chains and (b) the model red chains. The electron density is visualized in red for a hole fixed at the position indicated by a blue sphere.

Fig. 3. Figure 7(a) visualizes the computed dispersion for the example case of the model blue chains, highlighting the resulting stop-band of 2.23 eV. The Δ values obtained for all studied systems are summarized in Table II, and the experimental values are given for comparison. It should be emphasized that the effect of exciton dispersion on the polariton states of these systems is negligible. As outlined in Appendix B, the bandwidth of the exciton is equal to 1.33 eV from the zone center Γ ($|\mathbf{k}| = 0$) to the band-edge X ($|\mathbf{k}| = \frac{\pi}{\alpha}$ = 6.43 nm^{-1}) of the first Brillouin zone in the direction of the polymer chains. Within the same distance in momentum space, the energy of a photon changes by $\Delta E = \hbar c \frac{\pi}{\alpha} - 1.87 = 1,268$ eV, a change which is three orders of magnitude greater than that of the exciton energy.

We see from Table II that the model blue chains have significantly larger stop-band width than the model red system. Since the only difference between these structures is the torsional angle between subsequent diacetylene monomers (see Fig. 4), we conclude that the magnitude of this torsion has a strong effect on the magnitude of light–matter interactions. Indeed, the finite torsion of the model red system leads to deviations from the perfect dipole alignment of model blue PDA, which is crucial to facilitating strong coupling to photons. The computed values for the stop-band width are in reasonable agreement with the experimental values of Fig. 3, and the large difference between the blue and red structures is captured.
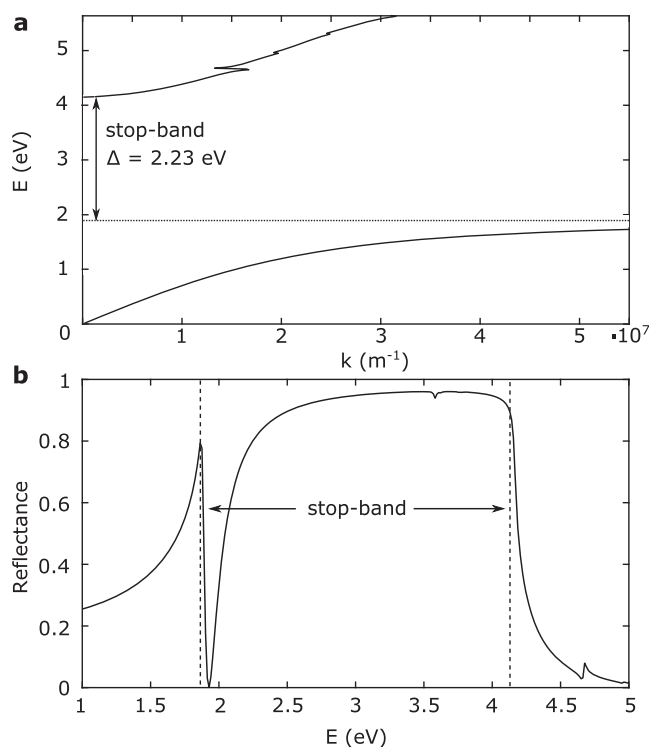
TABLE II. Values for the stop-band width of the four disorder-free PDA chains.

Structure	Δ (eV)—theory	Δ (eV)—experiment
Real blue	2.28	2.64
Model blue	2.23	. . .
Real red	1.06	1.16
Model red	1.45	. . .

Furthermore, the comparison of the predicted Δ values for the real and model red systems suggests that the introduction of polarizable side-chains leads to weaker exciton–photon interactions, closing the stop-band by almost 0.4 eV. This is likely due to two reasons. Firstly, the dielectric screening that they provide to electron–hole pairs (Fig. 6) leads to a more weakly bound exciton, which has a higher transition energy compared to the model system. Hence, the condition of Eq. (10) becomes more difficult to satisfy. This argument only holds for polarizable side-chains that provide significant screening, which is not the case for the real blue PDA. Indeed, the computed values of Δ for the real and model blue systems differ by a mere 50 meV. Moreover, upon the introduction of side-groups, a few exciton states with small but non-vanishing oscillator strength appear at energies above 3 eV, hence reducing the brightness of the main exciton peak according to the sum rule of Eq. (11) and also making the frequency range that satisfies the condition of Eq. (10) narrower.
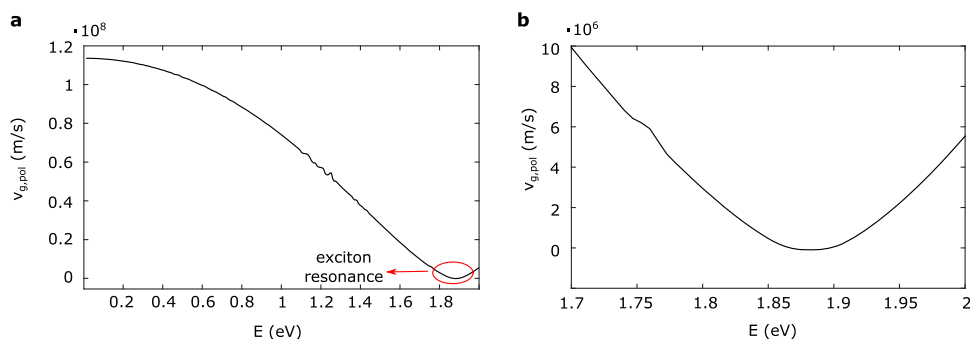
The values predicted by the calculations for the stop-band width are in reasonable agreement with experiment, as summarized in Table II. We believe that the differences are largely due to our modeling of a perfect periodic structure and ignoring exciton resonances which are present in a realistic film, for example, due to unpolymerized diacetylene monomers and minority chain populations at different geometries. Each of these weak transitions couples to photons and has a (narrow) stop-band of its own. The overlap of the different stop-bands due to the various weak exciton resonances with that of the main exciton peak leads to an overall wider stop-band.[4] In agreement with this line of thought, the predicted values underestimate experiment for both materials. It is, however, worth pointing out that while the overall stop-band is wider due to the presence of additional resonances, the individual stop-bands become narrower. This effect is discussed later and visualized in Fig. 12 for the main exciton peak in the presence of vibronic resonances.

For normal incidence of light, the reflectance can be calculated as

$$R(\omega) = \frac{(n(\omega) - 1)^2}{(n(\omega) + 1)^2}, \tag{13}$$

where $n(\omega)$ the complex refractive index of the material. For the model blue chains, this is plotted in Fig. 7(b), where the stop-band is clearly resolved. The absorption from the exciton state results in a low-reflectance gap within the stop-band, which is in agreement with experiment. However, the computed reflectivity spectrum looks qualitatively very different from the experimental one of Fig. 3(a). This is due to entirely ignoring the effects of disorder in the calculation. The presence of minority chain populations with different geometries, as well as unpolymerized diacetylene monomers,

FIG. 7. Calculated (a) polariton dispersion and (b) reflectance of the model blue PDA chains, highlighting the stop-band of width Δ = 2.23 eV.

FIG. 8. Polariton group velocity in model blue chains, for different energies of the incident light. Panel (a) shows a large region of frequencies and panel (b) provides a closer view of the region close to the resonance with the exciton.

is ignored, and the exciton states associated with these would lead to more gaps in the reflectivity. For the model chains, we ignore excitons associated with the side-chains, which would also introduce additional structure within the stop-band. We will see later that dynamic disorder is another important factor toward determining the internal structure of the stop-band.

Before moving on to consider the effects of disorder, we would like to comment on the speed of energy transfer in these materials, as predicted by the results of this section. First, let us consider the case of purely excitonic motion. The quantity that we need to compute in order to quantify the speed of band-like exciton motion is the exciton group velocity,

$$v_{g,exc} = \frac{1}{\hbar} \cdot \frac{\partial E_{exc}}{\partial q}, \tag{14}$$

where E_{exc} is the exciton energy and q is the exciton wavenumber. Following photoexcitation, a wavepacket is generated on the exciton potential energy surface, the momentum of which is narrowly distributed around $q = 0$, since light induces close-to-vertical transitions within the Franck-Condon approximation. The center of mass of this Γ-point exciton will then travel with the velocity of equation (14). We are interested in energy transfer in the direction of the chains, which we define to lie along the x axis, and we, thus, approximate $v_{g,exc}$ as the average along the respective dimension of reciprocal space. To this end, we calculate the exciton energy at the band-edge X, using a supercell calculation that is outlined in Appendix B, and we obtain

$$v_{g,exc} \approx \frac{1}{\hbar} \cdot \frac{E_{exc}(X) - E_{exc}(\Gamma)}{q(X) - q(\Gamma)} = 3 \cdot 10^5 \, m/s. \tag{15}$$

Now let us consider the group velocity of a polariton $v_{g,pol}$ close to the exciton resonance, which can be computed from the solution of Eq. (12) for different energies of the incident light. The result for the model blue chains is given in Fig. 8(a); at low frequencies, the speed of light propagating along the PDA chains is $c = c_o/n_{xx}$. However, as we approach the energy of the exciton transition, the exciton content of the lower polariton state becomes larger, reducing the speed of propagation. Figure 8(b) provides a closer view to the region around resonance, and we find that the polariton propagates with a speed of the order of 10^6 m/s, which is an order of magnitude faster than purely excitonic band-like propagation. One might observe that very close to the exciton resonance the group velocity obtains negative values, which is unphysical. This is due to the fact that in this

narrow region, the material exhibits anomalous dispersion and the group velocity is generally not a useful concept in these cases.[43]

IV. STATIC DISORDER: THE EFFECT OF FINITE CHAIN LENGTH

In a realistic film of PDA, the system deviates from the perfectly periodic behavior in more than one way. As we saw when discussing the experimental reflectivity spectra, unpolymerized chains of diacetylene can be present, as well as minority populations of chains at different conformations. Imperfections in the chain polymerization can lead to breaks in the conjugation of the system, or even to the termination of the polymer structure after a finite number of monomers. Here, we consider such effects limiting the chain conjugation, and we ignore atomic defects and vacancies, due to the pure character of the samples as discussed previously.

In order to understand the impact of finite conjugation lengths on the exciton and polariton properties, we study five different finite systems consisting of one to five diacetylene monomers, which we terminate on both sides with hydrogen atoms. For simplicity, we choose to terminate the chains after the occurrence of a triple bond so that the carbon atoms at the boundaries only need to bond with a single hydrogen. As an example, Fig. 9 visualizes a trimer of diacetylene.

We perform GW-BSE calculations on these oligomers, introducing a vacuum of 20 Å between their periodic images. We, thus, obtain $\varepsilon(\omega)$ for each of these and, similar to Sec. III, compute the energy of the first singlet exciton $E(S_1)$ and the stop-band width Δ, which we visualize in Figs. 10(a) and 10(b), respectively. We have chosen to construct the oligomer chains so that they are planar, and
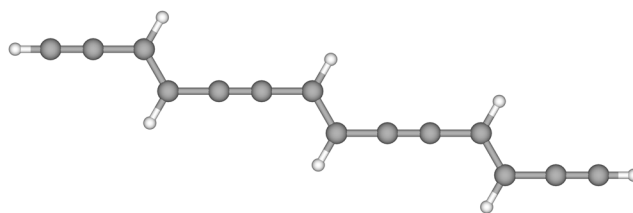
FIG. 9. A hydrogen-terminated trimer of diacetylene.
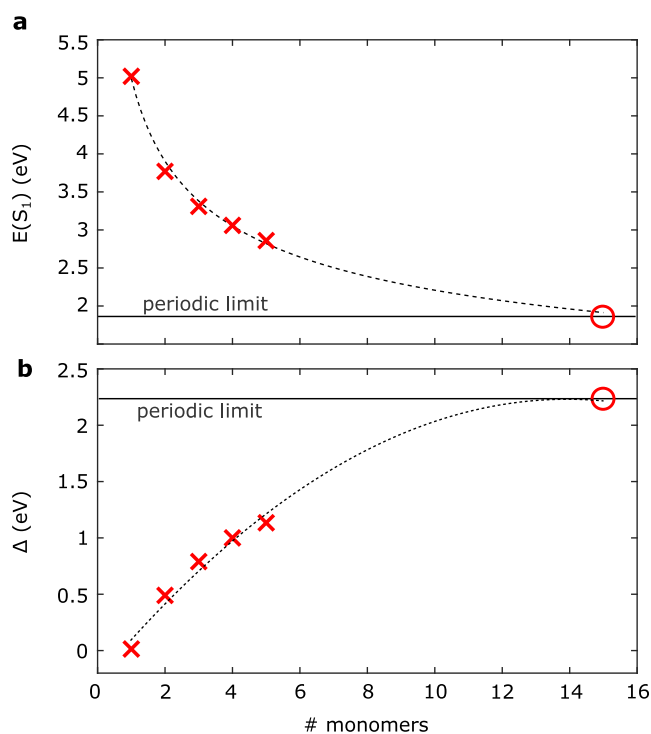
FIG. 10. The exciton energy [panel (a)] and stop-band width [panel (b)] for chains consisting of a different number of diacetylene monomers N. Since the constructed oligomers are planar, the periodic limit of the model blue chains is approached for a larger number of monomers.

hence by increasing the number of monomers, we approach the periodic limit of the model blue PDA chains of Sec. III, which is also noted on Fig. 10.

First of all, it is clear from Fig. 10(a) that as we add more monomers to the chain, the exciton energy is stabilized and converges to the periodic limit. Due to the large computational cost, we were unable to add the required number N of diacetylene monomers in order to reach the periodic limit; however, by performing model fits to the first five datapoints of Figs. 10(a) and 10(b) (dashed line), we estimate that the periodic limit is obtained for $N = 13$–15 monomers, in very close agreement with a previous experimental study.[57] Furthermore, we find that the stop-band width increases with a larger number of monomers in Fig. 10(b), and the periodic limit of an infinite chain provides the maximal possible magnitude for light–matter interactions. This can be rationalized from the fact that the exciton frequency appearing in the oscillator strength condition (10) decreases with increasing number of diacetylene monomers.

We, therefore, conclude that the presence of static disorder, in this case in the form of finite chain lengths, reduces the magnitude of light–matter interactions. However, the large measured stop-band width of $\Delta = 2.64$ eV for the blue chains suggests that conjugation-limiting effects are not important in PDA. Naturally, breaks in the conjugation and imperfect polymerization do occur; however, the results suggest that the vast majority of chains extend beyond

15 diacetylene monomers, for which number the periodic limit is reached, and the maximal light–matter coupling is obtained. Here, we do not compute the effect of static disorder on the reflectance of PDA, as this would require explicit inclusion of, for example, unpolymerized diacetylene monomers within a supercell of PDA, making the cost of these calculations prohibitive. We now proceed to discuss the effects of dynamic disorder on light–matter coupling.

V. DYNAMIC DISORDER: THE EFFECT OF VIBRATIONS

A purely electronic structure calculation predicts that there is only a single bright exciton state in PDA, the vertical transition peak in the computed absorption spectrum of Fig. 5. In reality, the ground- and excited-state potentials of the PDA chains are displaced along coupled vibrational normal modes, and electronic excitations involve multiple ending vibrational levels (and a thermalized distribution of starting vibrational levels). This is evident in the experimental absorption spectra of Fig. 3, where one can resolve vibrationally dressed 0–1 and 0–2 phonon side bands on top of the purely 0–0 electronic transition. Intuitively, it is obvious that these phonon side bands in the structure of $\mathrm{Im}(\varepsilon(\omega))$ will give rise to more structure in $\mathrm{Re}(\varepsilon(\omega))$ compared to the case of a single exciton peak, according to the following Kramers–Kronig relation:

$$\mathrm{Re}(\varepsilon(\omega)) = P \int_0^{+\infty} \frac{d\nu}{\pi} \mathrm{Im}(\varepsilon(\nu)) \frac{2\nu}{\nu^2 - \omega^2}. \tag{16}$$

This effect reduces the width of the region in which $\mathrm{Re}(\varepsilon(\omega)) < 0$ following an excitonic transition, as we show in Fig. 11(b). We call the width of this region Δ_{vib}, and the fact that it is smaller than Δ means that a gap in the high reflectivity of the stop-band is introduced [see Fig. 11(c)]. We, therefore, proceed to study the effects of exciton–phonon coupling, as a means of understanding the internal structure of the stop-band. To this end, we employ the linear-vibronic Hamiltonian[58]

$$H = \mathrm{E}(\mathrm{S_1}) \cdot I + \sum_k \hbar\omega_k \lambda_k \left(b_k^\dagger + b_k \right) + \sum_k \hbar\omega_k b_k^\dagger b_k, \tag{17}$$

where I is the identity and k runs over the phonon modes of the system, which have frequencies of ω_k. The energy of the first singlet exciton refers to the infinite periodic limit. The Huang-Rhys factors are calculated as

$$\lambda_k^2 = \left(\frac{\mathrm{V}_{\mathrm{ep},k}}{\hbar\omega_k} \right)^2, \tag{18}$$

where we approximate the first derivative $\mathrm{V}_{\mathrm{ep},k}$ of the exciton energy along mode k using the finite difference formula

$$\mathrm{V}_{\mathrm{ep},k} = \frac{\mathrm{E}(\mathrm{S_1})_{+\delta u(k)} - \mathrm{E}(\mathrm{S_1})_{-\delta u(k)}}{2\delta u(k)}, \tag{19}$$

with $\delta u(k)$ being a small dimensionless displacement along mode k. At a practical level, the calculation of $\mathrm{V}_{\mathrm{ep},k}$ requires two GW-BSE calculations at the displaced configurations of each mode, and constitutes a very computationally intensive process. We were, therefore, only able to obtain a full parameterization of the Hamiltonian (17) for the two model chains, which only have a small number of phonon modes due to the small size of their unit cell (18 and 36 modes for the model blue and red chains, respectively). The
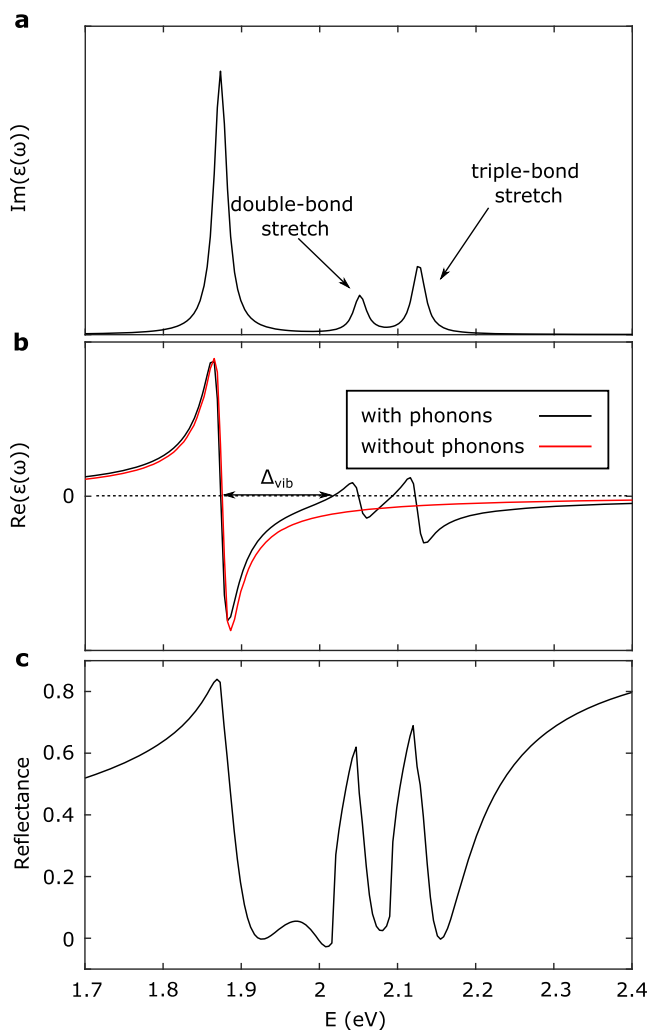
FIG. 11. The imaginary part [panel (a)] and real part [panel (b)] of the dielectric response of the model blue chains, once the effect of phonons is accounted for. The main extra contributions to the structure of $\varepsilon(\omega)$, compared to the disorder-free case, arise due to the effect of the carbon–carbon double- and triple-bond stretch. Comparing the structure of $\mathrm{Re}(\varepsilon(\omega))$ for the cases with and without phonons, we find that dynamic disorder leads to "breaks" within the region of $\mathrm{Re}(\varepsilon(\omega)) < 0$. This leads to a richer structure for the reflectance in panel (c), compared to the disorder-free case of Fig. 7.

existence of the side-chains for the real PDAs, for which we previously calculated the exciton properties, makes the task of computing exciton–phonon interactions a very formidable one, and we, thus, limit the following analysis to the model chains.

When computing the Huang-Rhys factors of PDA, one needs to account for the fact that the exciton can travel a finite distance of N monomers coherently, before being scattered by a phonon. Therefore, if $\lambda_{k,\mathrm{unit}}$ is the value obtained within a unit cell exciton calculation where the phonon mode k has been displaced, then the actual value of the Huang-Rhys parameter is[59]

$$\lambda_k^2 = \frac{\lambda_{k,\mathrm{unit}}^2}{N}. \tag{20}$$

We estimate the exciton coherence length N as

$$N = \frac{v_{\mathrm{g,exc}} \cdot \tau_{\mathrm{scatter}}}{L_{\mathrm{DA}}}, \tag{21}$$

where $v_{\mathrm{g,exc}}$ is the exciton group velocity from Sec. III, τ_{scatter} is the timescale for the exciton to be scattered by a phonon, and L_{DA} is the length of a single diacetylene monomer. Since we find that the excited state surface of the double-bond stretch is the steepest, that is, having the largest value of $V_{\mathrm{ep},k}$, we approximate τ_{scatter} by the period of 23 fs of this mode, giving us an exciton coherence length of $N = 15$ monomers for both model chains, in good agreement with previous estimates on similar systems.[28]

We write the ith eigenstate of the Hamiltonian of Eq. (17) as

$$|\Psi^{(i)}\rangle = \sum_{k=1}^{M} \sum_{\tilde{v}}^{N_q} c_{\tilde{v}_k}^{(i)} |1, \tilde{v}_k\rangle, \tag{22}$$

where there are M vibrational modes in total. The basis state $|1, \tilde{v}_k\rangle$ is the short-hand notation for

$$|1, \tilde{v}_k\rangle = |1, 0, 0, \ldots, \tilde{v}_k, 0, \ldots, 0\rangle, \tag{23}$$

that is, the state where the exciton is populated and the first index set to one, and where among all vibrational modes, only mode k is populated by $\tilde{v}_k$ quanta. We, thus, only allow a single mode to be excited at one time, as a means of simplifying the problem. In principle, every phonon mode can admit an infinite number of quanta; however, in practice we need to truncate the associated Hilbert space to only allow for up to N_q quanta in each mode. We find that for the model PDA chains $N_q = 3$ converges the results for the dielectric response.

Similar to previous works,[58] we include the effect of vibrations in the absorption spectrum by taking

$$\mathrm{Im}(\varepsilon(\omega)) = (c_0^{(1)})^2 \cdot \mathrm{Im}(\varepsilon(\omega))_{0-0}$$
$$+ \left| \sum_k \sum_{\tilde{v}} c_{\tilde{v}_k}^{(1)} \frac{\lambda_k^{2\tilde{v}_k} e^{-\lambda_k^2}}{\tilde{v}_k!} \right|^2 W(\omega - \omega_{\mathrm{S}_1} - \omega_k), \tag{24}$$

where $W(\omega - \omega_{\mathrm{S}_1} - \omega_k)$ is a Lorentzian centered around $\omega_{\mathrm{S}_1} + \omega_k$, for which we use the same width as for the peaks of the purely electronic part $\mathrm{Im}(\varepsilon(\omega))_{0-0}$ of the dielectric response, as obtained from GW-BSE calculations detailed in Appendix B. Moreover, in Appendix B, we show for the example case of the model blue chains that the result for the width Δ_{vib} is largely independent of the peak width γ for values of γ between 5 meV and 50 meV. The coefficients $c^{(1)}$ are obtained by diagonalizing the Hamiltonian (17), with $c_0^{(1)}$ denoting the contribution from the purely excitonic basis state $|1, 0, 0, \ldots, 0\rangle$. Here, we reside to approximating the absorbance $\alpha(\omega)$ with $\mathrm{Im}(\varepsilon(\omega))$. This is a reasonable approximation for determining Δ_{vib} since this quantity depends on the intensity ratio of the peaks 0–0, 0–1, 0–2, etc. The absorbance $\alpha(\omega)$ and imaginary dielectric response $\mathrm{Im}(\varepsilon(\omega))$ are proportional to each other, which suggests that the error we introduce is small.

For the example case of the model blue chains, we visualize the result of including phonon effects on $\mathrm{Im}(\varepsilon(\omega))$ in Fig. 11(a), while Fig. 11(b) shows the corresponding $\mathrm{Re}(\varepsilon(\omega))$ as obtained by

using the Kramers–Kronig relation (16). For $Re(\varepsilon(\omega))$, we also draw a comparison to the case without phonons. The peaks that feature prominently in the absorption spectrum are due to the double- and triple-bond carbon stretching motions, with energies of 0.18 eV and 0.26 eV, respectively. Indeed, in the experimental absorption spectrum of the blue PDA in Fig. 3(a), two vibronic peaks feature prominently at energies of 0.19 eV and 0.25 eV above the main exciton peak; however, their relative intensity is opposite to the computed one. Intuitively, one can understand why the double-bond and triple-bond vibrations are most strongly coupled to the exciton from the fact that they transiently lead to structures with a smaller bond-length alternation, i.e., deviating from the Peierls-distorted structure that gives conjugated polymers such as PDA their semiconducting character, and bring the material closer to the metallic limit.[60] It is hence not surprising that these motions have a large effect on the optical properties of the studied PDAs. This also suggests that the coupling to these motions is extremely sensitive to the precise bond-length alternation of the PDA backbone, potentially accounting for the discrepancy between the theoretical and experimental absorption spectra when it comes to their relative importance. For the computed exciton coherence length of $N = 15$, we obtain Δ_{vib} values of 137 meV and 123 meV for the model blue and the model red chains, respectively. We compute the associated reflectivity spectra in Fig. 11(c), where we find that vibronic peaks introduce "gaps" within the high reflectance region of the stop-band.

Therefore, accounting for vibrational effects allows one to predict part of the internal structure of the stop-band of an exciton that is strongly coupled to a photon. However, the precise form of the reflectivity, depends very sensitively on the exciton coherence length N, as shown in Fig. 12, where we use the width Δ_{vib} as a proxy for the size of phonon-induced gaps in the reflectivity. This dependence of Δ_{vib} on N enters through the Huang-Rhys factors of the extended system; see Eq. (20). In turn, the exciton coherence length depends on the exciton group velocity and the period of phonon modes, as seen in Eq. (21). Hence, the interplay of phonons with excitons is established to be crucial for the interaction of the latter with light.
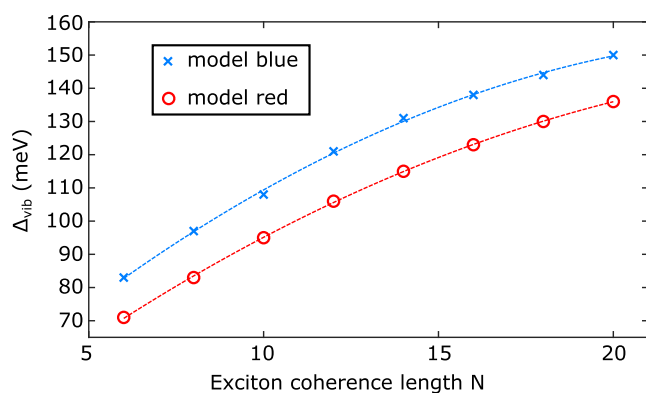
FIG. 12. The dependence of the width Δ_{vib} of the two model PDA chains, on the exciton coherence length.

VI. CONCLUSIONS

In this work, we have presented a theoretical framework for obtaining the properties of exciton-polaritons in organic materials. Our approach requires input from a calculation of the material's dielectric response and is agnostic to the methodology used to obtain it. By employing *GW*-BSE calculations for the electronic structure of polydiacetylenes, we obtain their stop-band width, which characterizes the strength of light–matter interactions. The results are in reasonable agreement with experiment, and we attribute the differences to our treatment of the materials as perfectly periodic, neglecting effects of disorder and additional excitons that weakly couple to light. We compute the speed of propagation of a polariton close to the resonance of light with an exciton, showing that this is an order of magnitude faster than purely excitonic motion. We find the conjugation length of polymer chains to be a critical parameter toward determining the magnitude of light–matter interactions, highlighting one manifestation of how static disorder can lead to weaker exciton–photon coupling. This effect is not important for the polydiacetylenes studied here, due to the purity of these materials. It could, however, be of relevance for different systems. Furthermore, we discuss the important role of dynamic disorder and show that vibrational effects introduce gaps within the frequency range of large reflectance that characterizes polaritons. We also discuss the screening of the Coulomb interaction provided by the side-chains of polydiacetylene as another potentially important contribution toward determining the magnitude of light–matter interactions. Thus, all of the aforementioned factors appearing in realistic materials are important toward an accurate description of exciton–photon coupling. In principle, one needs to account for the above factors at the same time and self-consistently, something which is computationally challenging and will be the subject of a future work.

APPENDIX A: EXPERIMENTAL REFLECTIVITY MEASUREMENTS

Microscopic transmission and reflectance measurements were performed using a Zeiss AxioScope optical microscope in Köhler illumination equipped with a 100× objective (Zeiss EC Epiplan-APOCHROMAT 0.95 HD DIC) coupled to a spectrometer (Avantes

HS2048) via an optical fiber (Thorlabs, FC-UV50-2-SR). Five spectra were collected for each sample using an integration time of 10 ms and 20 ms for reflection and transmission measurements, respectively. The reflectance and transmittance were calculated using a silver mirror (Thorlabs, PF10-03-P01) and the glass substrate as references, respectively.

APPENDIX B: COMPUTATIONAL DETAILS

1. Electronic structure calculations

We perform density functional theory (DFT) calculations using the Quantum Espresso software package,[61] with the PBE functional together with a 60 Ry plane wave cutoff energy. For the model blue and model red chains, we employ $8 \times 4 \times 2$ and $4 \times 4 \times 2$ **k**-point grids, respectively. For the real red chains, we use $4 \times 4 \times 2$, and for the real blue system $4 \times 2 \times 4$. For the model PDAs, we introduce a vacuum of 10 Å between neighboring polymer chains, in order to minimize inter-chain interactions.

We perform energy self-consistent GW calculations (i.e., GW_0) using the YAMBO code.[62] For the real chains, we find that including 400 Kohn-Sham states, 300 bands for the calculation of the polarization function, and a 7 Ry cutoff for the dielectric matrix leads to converged values for the quasiparticle bandgaps. For the model blue (red) chains, we use 40 (80) Kohn-Sham states, 40 (80) bands for the calculation of the polarization function, and a 3 Ry cutoff for the dielectric matrix.

We solve the Bethe–Salpeter equation for the model blue (red) PDA using 4 (8) occupied and 4 (8) unoccupied bands, converging the position of the first exciton peak. For the exchange term in the Bethe–Salpeter kernel, the cutoff is set to 60 Ry. For the real chains, we use 10 occupied and 10 unoccupied bands and set the exchange to 40 Ry. In order to emulate the experimental conditions, the incident electric field is chosen to lie in the direction of the polymer chains. The imaginary part of $\varepsilon(\omega)$ is obtained by fitting a Lorentzian of 10 meV width to the computed excitonic eigenvalues of the BSE Hamiltonian. The broadening of the absorption spectrum due to vibrational effects as presented in Fig. 11 is then added on top of that, along with the additional peaks.

Due to the one-dimensional character of the model PDAs, divergences can occur at small values of q (i.e., at long distances) in the Coulomb term that appears in the many-body calculations. In order to avoid this problem, we use the random integration method, as implemented in YAMBO. We converge the calculations using 10^5 random q-points in the first Brillouin zone and by setting the cutoff for the real space components of the Coulomb interaction to 20 Ry.

For the model PDAs, we estimate the dispersion of the exciton band along $\Gamma - X$ as follows. We generate a supercell of size $2 \times 1 \times 1$, thus halving the size of the first Brillouin zone. As a result, the zone-boundary X point folds onto Γ, which appears as an extra exciton state once the BSE Hamiltonian of the $2 \times 1 \times 1$ system is diagonalized. The distance of this new band from the exciton value at Γ gives the width of the exciton band, which we find to be equal to 1.33 eV.

The aforementioned electronic structure calculations are performed on the PDA structures as obtained from X-ray diffraction

(for the real systems). For the model systems, calculations are performed on the structures as obtained from X-ray diffraction and following the substitution of the side-chains with hydrogen atoms. Due to the extreme sensitivity of the computed exciton properties on the bond-length alternation (BLA) of the polymer chain, we set the BLA of the blue chains to be exactly identical to that of the red chains, in order to focus on the effects of the relative torsion between diacetylene monomers and on the screening effect provided by the side-chains. A geometry optimization of these structures is not carried out, as the BLA of these one-dimensional carbon chains is known to be extremely sensitive to the fraction of exact exchange that the employed DFT functional includes.[63] It has been shown that while hybrid functionals perform better than the generalized gradient approximation (GGA),[63] it is necessary to use very accurate methods such as Quantum Monte Carlo in order to obtain geometries with realistic BLAs, which is beyond the scope of this work. Since the exciton energy is extremely sensitive to the precise value of the BLA, we limit ourselves to obtaining exciton energies for unoptimized structures and only optimize the geometry of the studied structures prior to phonon calculations.

2. Phonon calculations

We calculate the lattice dynamics of the different PDA variants in the harmonic approximation using finite differences.[41,42] We calculate the dynamical matrix on a $1 \times 1 \times 1$ coarse **q**-point grid. Therefore, we only account for the effect of Γ-point phonons, which provides a good approximation, since these are most strongly coupled to the zero-momentum exciton states that result from photoexcitation. Prior to phonon calculations, the geometry of the different PDAs is optimized using the PBE functional.

3. Dependence of polariton splitting on peak width

Figure 13 visualizes the value of Δ_{vib} of the model blue PDA, within a range of values for the width of the exciton and vibronic peaks, ranging from 5 meV to 50 meV. We find that Δ_{vib} does not vary by more than 10 meV within this range of widths. Here, an exciton coherence length $N = 15$ has been used.
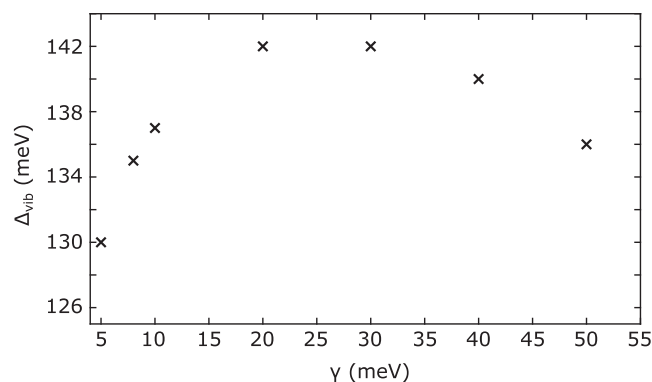

FIG. 13. The dependence of the width Δ_{vib} of the first region with $Re(\varepsilon(\omega))$ on the width γ of the exciton and vibronic peaks.

DATA AVAILABILITY

The data underlying this publication can be found in https://doi.org/10.17863/CAM.56203.

REFERENCES

[1] S. I. Pekar, "The theory of electromagnetic waves in a crystal in which excitons are produced," Sov. J. Exp. Theor. Phys. **6**(4), 785 (1958).

[2] S. I. Pekar, "Identification of excitons with light waves in a crystal," Sov. J. Exp. Theor. Phys. **11**(6), 1286 (1960).

[3] J. J. Hopfield, "Theory of the contribution of excitons to the complex dielectric constant of crystals," Phys. Rev. **112**(5), 1555–1567 (1958).

[4] H. Kalt and C. F. Klingshirn, *Semiconductor Optics 1*, 5th ed. (Springer, 2019), Chap. 8.

[5] S. Reineke, F. Lindner, G. Schwartz, N. Seidler, K. Walzer, B. Lüssem, and K. Leo, "White organic light-emitting diodes with fluorescent tube efficiency," Nature **459**(7244), 234–238 (2009).

[6] L. Meng, Y. Zhang, X. Wan, C. Li, X. Zhang, Y. Wang, X. Ke, Z. Xiao, L. Ding, R. Xia, H. L. Yip, Y. Cao, and Y. Chen, "Organic and solution-processed tandem solar cells with 17.3% efficiency," Science **361**(6407), 1094–1098 (2018).

[7] A. Strashko, P. Kirton, and J. Keeling, "Organic polariton lasing and the weak to strong coupling crossover," Phys. Rev. Lett. **121**(19), 193601 (2018).

[8] S. Kéna-Cohen and S. R. Forrest, "Room-temperature polariton lasing in an organic single-crystal microcavity," Nat. Photonics **4**(6), 371–375 (2010).

[9] M. Knupfer, "Exciton binding energies in organic semiconductors," Appl. Phys. A **77**(5), 623–626 (2003).

[10] A. Köhler and H. Bässler, "Triplet states in organic semiconductors," Mater. Sci. Eng. R: Rep. **66**(4-6), 71–109 (2009).

[11] D. Beljonne, H. Yamagata, J. L. Brédas, F. C. Spano, and Y. Olivier, "Charge-transfer excitations steer the Davydov splitting and mediate singlet exciton fission in pentacene," Phys. Rev. Lett. **110**(22), 226402 (2013).

[12] T. C. Berkelbach, M. S. Hybertsen, and D. R. Reichman, "Microscopic theory of singlet exciton fission. II. Application to pentacene dimers and the role of superexchange," J. Chem. Phys. **138**(11), 114103 (2013).

[13] S. R. Yost, J. Lee, M. W. B. Wilson, T. Wu, D. P. McMahon, R. R. Parkhurst, N. J. Thompson, D. N. Congreve, A. Rao, K. Johnson, M. Y. Sfeir, M. G. Bawendi, T. M. Swager, R. H. Friend, M. A. Baldo, and T. Van Voorhis, "A transferable model for singlet-fission kinetics," Nat. Chem. **6**(6), 492–497 (2014).

[14] P. B. Coto, S. Sharifzadeh, J. B. Neaton, and M. Thoss, "Low-lying electronic excited states of pentacene oligomers: A comparative electronic structure study in the context of singlet fission," J. Chem. Theory Comput. **11**(1), 147–156 (2015).

[15] M. Litinskaya, P. Reineker, and V. M. Agranovich, "Exciton-polaritons in organic microcavities," J. Lumin. **119-120**, 277–282 (2006).

[16] D. G. Lidzey, D. D. C. Bradley, M. S. Skolnick, T. Virgili, S. Walker, and D. M. Whittaker, "Strong exciton-photon coupling in an organic semiconductor microcavity," Nature **395**(6697), 53–55 (1998).

[17] D. Polak, R. Jayaprakash, T. P. Lyons, L. Á. Martínez-Martínez, A. Leventis, K. J. Fallon, H. Coulthard, D. G. Bossanyi, K. Georgiou, A. J. Petty II, J. Anthony, H. Bronstein, J. Yuen-Zhou, A. I. Tartakovskii, J. Clark, and A. J. Musser, "Manipulating molecules with strong coupling: Harvesting triplet excitons in organic exciton microcavities," Chem. Sci. **11**(2), 343–354 (2020).

[18] V. M. Agranovich, M. Litinskaia, and D. G. Lidzey, "Cavity polaritons in microcavities containing disordered organic semiconductors," Phys. Rev. B **67**(8), 085311 (2003).

[19] A. Canaguier-Durand, C. Genet, A. Lambrecht, T. W. Ebbesen, and S. Reynaud, "Non-Markovian polariton dynamics in organic strong coupling," Eur. Phys. J. D **69**(1), 24 (2015).

[20] T. W. Ebbesen, "Hybrid light-matter states in a molecular and material science perspective," Acc. Chem. Res. **49**(11), 2403–2412 (2016).

[21] A. Troisi, G. Orlandi, and J. E. Anthony, "Electronic interactions and thermal disorder in molecular crystals containing cofacial pentacene units," Chem. Mater. **17**(20), 5024–5031 (2005).

[22] A. Troisi and G. Orlandi, "Dynamics of the intermolecular transfer integral in crystalline organic semiconductors," J. Phys. Chem. A **110**(11), 4065–4070 (2006).

[23] P. Cudazzo, F. Sottile, A. Rubio, and M. Gatti, "Exciton dispersion in molecular solids," J. Phys.: Condens. Matter **27**(11), 113204 (2015).

[24] S. Refaely-Abramson, F. H. Da Jornada, S. G. Louie, and J. B. Neaton, "Origins of singlet fission in solid pentacene from an ab initio Green's function approach," Phys. Rev. Lett. **119**(26), 267401 (2017).

[25] A. M. Alvertis, R. Pandya, L. A. Muscarella, N. Sawhney, M. Nguyen, B. Ehrler, A. Rao, R. H. Friend, A. W. Chin, and B. Monserrat, "The impact of exciton delocalization on exciton-vibration interactions in organic semiconductors," arXiv:2006.03604, 2020.

[26] R. F. Mahrt and H. Bässler, "Light and heavy excitonic polarons in conjugated polymers," Synth. Met. **45**(1), 107–117 (1991).

[27] F. C. Spano, "The spectral signatures of Frenkel polarons in H- and J-aggregates," Acc. Chem. Res. **43**(3), 429–439 (2010).

[28] H. Yamagata and F. C. Spano, "Vibronic coupling in quantum wires: Applications to polydiacetylene," J. Chem. Phys. **135**(5), 054906 (2011).

[29] N. Somaschi, L. Mouchliadis, D. Coles, I. E. Perakis, D. G. Lidzey, P. G. Lagoudakis, and P. G. Savvidis, "Ultrafast polariton population build-up mediated by molecular phonons in organic microcavities," Appl. Phys. Lett. **99**(14), 143303 (2011).

[30] N. Wu, J. Feist, and F. J. Garcia-Vidal, "When polarons meet polaritons: Exciton-vibration interactions in organic molecules strongly coupled to confined light fields," Phys. Rev. B **94**(19), 195409 (2016).

[31] D. M. Coles, P. Michetti, C. Clark, W. C. Tsoi, A. M. Adawi, J.-S. Kim, and D. G. Lidzey, "Vibrationally assisted polariton-relaxation processes in strongly coupled organic-semiconductor microcavities," Adv. Funct. Mater. **21**(19), 3691–3696 (2011).

[32] J. Del Pino, F. A. Y. N. Schröder, A. W. Chin, J. Feist, and F. J. Garcia-Vidal, "Tensor network simulation of polaron-polaritons in organic microcavities," Phys. Rev. B **98**(16), 165416 (2018).

[33] J. Del Pino, F. A. Y. N. Schröder, A. W. Chin, J. Feist, and F. J. Garcia-Vidal, "Tensor network simulation of non-Markovian dynamics in organic polaritons," Phys. Rev. Lett. **121**(22), 227401 (2018).

[34] H. Haug and S. W. Koch, *Quantum Theory of the Optical and Electronic Properties of Semiconductors*, 4th ed. (World Scientific, 2004), Chap. 11.

[35] F. A. Y. N. Schröder, D. H. P. Turban, A. J. Musser, N. D. M. Hine, and A. W. Chin, "Tensor network simulation of multi-environmental open quantum dynamics via machine learning and entanglement renormalisation," Nat. Commun. **10**(1), 1062 (2019).

[36] A. M. Alvertis, F. A. Y. N. Schröder, and A. W. Chin, "Non-equilibrium relaxation of hot states in organic semiconductors: Impact of mode-selective excitation on charge transfer," J. Chem. Phys. **151**(8), 084104 (2019).

[37] H. Lars, "New method for calculating the one-particle Green's function with application to the electron-gas problem," Phys. Rev. **139**(17), 796–823 (1965).

[38] M. Rohlfing and S. G. Louie, "Electron-hole excitations in semiconductors and insulators," Phys. Rev. Lett. **81**(11), 2312–2315 (1998).

[39] M. Rohlfing and S. G. Louie, "Electron-hole excitations and optical spectra from first principles," Phys. Rev. B **62**(8), 4927–4944 (2000).

[40] M. Rohlfing and S. G. Louie, "Optical excitations in conjugated polymers," Phys. Rev. Lett. **82**(9), 1959 (1999).

[41] K. Kunc and R. M. Martin, "*Ab initio* force constants of GaAs: A new approach to calculation of phonons and dielectric properties," Phys. Rev. Lett. **48**(6), 406–409 (1982).

[42] B. Monserrat, "Electron – phonon coupling from finite differences," J. Phys.: Condens. Matter **30**, 083001 (2018).

[43] J. D. Jackson, *Classical Electrodynamics*, 2nd ed. (Wiley, New York, London, 1975).

[44] S. Dai, Z. Fei, Q. Ma, A. S. Rodin, M. Wagner, A. S. McLeod, M. K. Liu, W. Gannett, W. Regan, K. Watanabe, T. Taniguchi, M. Thiemens, G. Dominguez, A. H. C. Neto, A. Zettl, F. Keilmann, P. Jarillo-Herrero, M. M. Fogler, and D. N. Basov, "Tunable phonon polaritons in atomically thin van der waals crystals of boron nitride," Science **343**(6175), 1125–1129 (2014).

[45] A. V. Zayats, I. I. Smolyaninov, and A. A. Maradudin, "Nano-optics of surface plasmon polaritons," Phys. Rep. **408**(3-4), 131–314 (2005).

[46] J. Lagois and B. Fischer, "Chapter 2 - surface exciton polaritons from an experimental viewpoint," in *Surface Polaritons, Modern Problems in Condensed Matter Sciences*, edited by D. L. Mills and V. M. Agranovich (North Holland Publishing Company: Sole distributors for the USA and Canada, Elsevier Science Publishing Company, Amsterdam, New York, 1982).

[47] M. Schott and G. Wegner, "Chapter III-1 - basic structural and electronic properties of polydiacetylenes, in *Nonlinear Optical Properties of Organic Molecules and Crystals*, edited by D. S. Chemla and J. Zyss (Academic Press, 1987), pp. 3–49.

[48] P. Spinat, C. Brouty, A. Whuler, and M. C. Sichère, "Determination structurale a 205 K du poly {bis [(p-bromophenylcarbamoyloxy)-4 butyl] - 1, 2 butene-1 yne-3 ylene}, $(C_{26}H_{26}Br_2N_{204})$ n," Acta Crystallogr. **41**, 1452–1455 (1985).

[49] V. Enkelmann and G. Schleier, "Poly[1,2-bis(diphenylaminomethyl)-1-buten-3-ynylene]," Acta Crystallogr., Sect. B: Struct. Sci., Cryst. Eng. Mater. **36**(8), 1954–1956 (1980).

[50] T. Barisien, L. Legrand, G. Weiser, J. Deschamps, M. Balog, B. Boury, S. G. Dutremez, and M. Schott, "Exciton spectroscopy of red polydiacetylene chains in single crystals," Chem. Phys. Lett. **444**(4-6), 309–313 (2007).

[51] M. Schott, "The colors of polydiacetylenes: A commentary," J. Phys. Chem. B **110**(32), 15864–15868 (2006).

[52] M. R. Philpott, "Optical reflection spectroscopy of organic solids," Annu. Rev. Phys. Chem. **31**, 97–129 (1980).

[53] S. C. J. Meskers and G. Lakhwani, "Reflection of light by anisotropic molecular crystals including exciton-polaritons and spatial dispersion," J. Chem. Phys. **145**(19), 194703 (2016).

[54] M. Tristani-Kendra, C. J. Eckhardt, J. Bernstein, and E. Goldstein, "Strong coupling in the optical spectra of polymorphs of a squarylium dye," Chem. Phys. Lett. **98**(1), 57–61 (1983).

[55] J.-S. Filhol, J. Deschamps, S. G. Dutremez, B. Boury, T. Barisien, L. Legrand, and M. Schott, "Polymorphs and colors of polydiacetylenes: A first principles study," J. Am. Chem. Soc. **131**(20), 6976–6988 (2009).

[56] A. Horvath, G. Weiser, C. Lapersonne-Meyer, M. Schott, and S. Spagnoli, "Wannier excitons and Franz-Keldysh effect of polydiacetylene chains diluted in their single crystal monomer matrix," Phys. Rev. B **53**(20), 13507–13514 (1996).

[57] F. Wudl and S. P. Bitler, "Synthesis and some properties of poly(diacety1ene) (polyenyne) oligomers," J. Am. Chem. Soc. **108**(15), 4685–4687 (1986).

[58] F. C. Spano, "Absorption and emission in oligo-phenylene vinylene nanoaggregates: The role of disorder and structural defects," J. Chem. Phys. **116**(13), 5877–5891 (2002).

[59] F. C. Spano and H. Yamagata, "Vibronic coupling in J-aggregates and beyond: A direct means of determining the exciton coherence length from the photoluminescence spectrum," J. Phys. Chem. B **115**(18), 5133–5143 (2011).

[60] S. Kivelson and A. J. Heeger, "First-order transition to a metallic state in polyacetylene: A strong-coupling polaronic metal," Phys. Rev. Lett. **55**(3), 308–311 (1985).

[61] P. Giannozzi, S. Baroni, N. Bonini, M. Calandra, R. Car, C. Cavazzoni, D. Ceresoli, G. L. Chiarotti, M. Cococcioni, I. Dabo, A. Dal Corso, S. De Gironcoli, S. Fabris, G. Fratesi, R. Gebauer, U. Gerstmann, C. Gougoussis, A. Kokalj, M. Lazzeri, L. Martin-Samos, N. Marzari, F. Mauri, R. Mazzarello, S. Paolini, A. Pasquarello, L. Paulatto, C. Sbraccia, S. Scandolo, G. Sclauzero, A. P. Seitsonen, A. Smogunov, P. Umari, and R. M. Wentzcovitch, "Quantum espresso: A modular and open-source software project for quantum simulations of materials," J. Phys.: Condens. Matter **21**(39), 395502 (2009).

[62] D. Sangalli, A. Ferretti, H. Miranda, C. Attaccalite, I. Marri, E. Cannuccia, P. Melo, M. Marsili, F. Paleari, A. Marrazzo, G. Prandini, P. Bonfà, M. O. Atambo, F. Affinito, M. Palummo, A. Molina-Sánchez, C. Hogan, M. Grüning, D. Varsano, and A. Marini, "Many-body perturbation theory calculations using the yambo code," J. Phys.: Condens. Matter **31**(32), 325902 (2019).

[63] E. Mostaani, B. Monserrat, N. D. Drummond, and C. J. Lambert, "Quasiparticle and excitonic gaps of one-dimensional carbon chains," Phys. Chem. Chem. Phys. **18**(22), 14810–14821 (2016).